Stealth and Bright Monomolecular Fluorescent Organic Nanoparticles Based on Folded Amphiphilic Polymer

Mayeul Collot, Jérémy Schild, Kyong T. Fam, Redouane Bouchaala, Andrey S. Klymchenko**

*Corresponding authors: mayeul.collot@unistra.fr; andrey.klymchenko@unistra.fr

Laboratoire de Bioimagerie et Pathologies, UMR 7021 CNRS, Faculté de Pharmacie, Université de Strasbourg, 74, Route du Rhin, 67401 Illkirch, France

Abstract

Fluorescent nanoparticles (NPs), owing to their superior brightness, are an attractive alternative to organic dyes. However, their cellular applications remain limited because of their large size, poor homogeneity and non-specific interactions in biological media. Herein, we propose a concept of monomolecular fluorescent organic nanoparticle of high brightness and very small size (10-14 nm) built of a single amphiphilic polymer bearing specially designed fluorescent dyes. We found that high PEGylation of poly(maleic anhydride-alt-1-octadecene (PMAO) favors a single-chain polymer folding into monomolecular stealth NPs with highly reduced non-specific interactions with live cells. To ensure high stability of our NPs, the fluorophores (BODIPYs) are covalently linked to the polymer through an optimized linker. Among tested linkers of different lengths and polarity, short medium-polar linker favoring location of the dyes at NPs interface ensures good

fluorescence quantum yield and small particle size. The fluorescence brightness of these NPs has been dramatically enhanced by increasing the bulkiness of the BODIPY dyes that prevents their *H*-aggregation, reaching 2,500,000 M^{-1} cm^{-1} (extinction coefficient × quantum yield). Fluorescence microscopy revealed that the single-particle brightness of these NPs is ~5-fold higher than that of QDot-585 using the same excitation wavelength (532 nm). Finally, when microinjected inside cells, these small and stealth NPs (10-nm diameter) distribute more evenly than 20-nm QDots inside the cytosol, showing similar spreading as a fluorescent protein. Thus, the developed monomolecular NPs, owing to small size and stealth properties, are artificial analogues of fluorescent proteins, surpassing the latter >50-fold in terms of brightness.

TOC Graphic

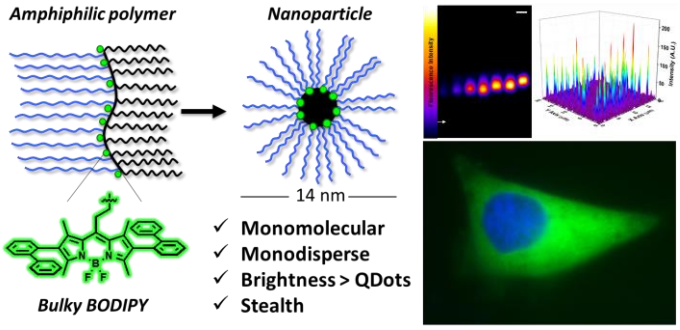

Keywords: amphiphilic polymer, fluorescent nanoparticles, single-chain polymer folding, aggregation-caused quenching, fluorescent dyes, fluorescence imaging, intracellular distribution

Fluorescent nanoparticles (NPs) attracted attention in the last decades due to their high brightness, equivalent to 10-100 organic dyes, and multi-functionality.[1,2] However, when it comes to replace organic dyes in cellular imaging applications, their relatively large size 30-300 nm poses serious limitations. Ideally, to study cellular processes at the molecular level, their size should not exceed that of biomolecules (5-15 nm), such as proteins and nucleic acids. First, the small size of NPs ensures minimal perturbation of the localization and function of the labeled biomolecules. Second, sizes below 20 nm are required for free diffusion of the particles in the highly crowded intracellular environment.[3,4] Third, small size will provide better localization precision in super-resolution imaging techniques, which now requires labels of sizes around 10 nm and below.[5] On the other hand, ultra-small NPs have been found promising for *in vivo* applications for both imaging and drug delivery applications, because of their higher capacity to penetrate into target tumors and their facilitated renal elimination.[6,7]

Among small-sized luminescent NPs, one should first mention QDs, having the fluorescent core of 4-7 nm and thin organic shell reported recently giving total diameter of QDs of 10-15 nm.[8-10] However, biocompatible coating in commercially available QDs is much thicker, so that the typical size of QDs is 20-30 nm. Similar characteristics can be considered for other systems based on the inorganic core NPs.[1] Dye-doped silica NPs with biocompatible shell can go down to 10 nm in size, although in this case the number of encapsulated dyes is limited.[11] Gold clusters[7,12] and carbon dots[13,14] featuring ultra-small size emerged recently, although their emission brightness and absorption characteristics need further improvement. Overall, inorganic nanoparticles feature rather limited and complex biodegradability profiles,[15] and they require organic shell for biocompatibility and bioconjugation. Organic NPs appear as very attractive alternative to inorganic NPs, because, on the one hand, their core can bear large number of dyes and, on the

other hand, their organic nature offer enormous chemical versatility for bio-functionalization and achieving biocompatibility, colloidal stability and potential biodegradability. Among organic NPs of ultrasmall size, one should mention those made of conjugated polymers[16-18] or organic dyes,[19,20] in particular aggregation-induced emission NPs,[21-23] and dye-loaded NPs build of polymers[23,24] and lipids.[25] Particularly fruitful approach to ultra-small NPs is based on self-assembly of organic dyes into micelles.[26-31] However, micelles are dynamic structures, so that to make them stable in biological systems these micelles are either assembled from polymers (polymeric micelles),[6,32,33] or the polymerization of micelles is done *in situ*.[28,29] An alternative approach that mimics micellar assembly is to directly use an amphiphilic polymer that can fold as a single molecule into a spherical nanoparticle, similar to the protein folding.[34,35] This process is known as single-chain polymer folding,[36-41] which has been successfully applied for generating small NPs by their assembly in water.[42-46] These systems has been already proposed for applications in catalysis,[47,48] especially catalytic nanoreactors[49] and artificial enzymes,[48,50] stimuli-responsive NPs,[51,52] and drug nanocarriers.[53] Fluorescent single-chain polymer nanoparticles is an emerging area of research,[54] with several examples reported in the recent literature.[46,52,55,56] Nevertheless, so far, it remains a challenge to obtain single-chain fluorescent NPs characterized by high brightness, comparable to QDs and at the same time displaying biocompatible surface for their cellular imaging applications.

Therefore, we turn our attention towards poly(maleic anhydride-alt-1-octadecene) (PMAO), which is a low-cost amphiphilic reactive polymer widely used to wrap nanocrystals[57] including QDs,[58-60] UCNPs,[61,62] metallic NPs[63] in order to make them water-soluble. [1] Despite its broad application for coating NPs, it has not been explored to generate single-chain fluorescent NPs. In one report, PMAO was used to form NPs, encapsulating non-covalently a fluorescent dye

(squaraine),[64] so the NPs were not based on a single molecule. Moreover, although small NPs (16.2 ± 6.1 nm) were initially obtained, glycol chitosan coating doubled the diameter to 32.5 ± 7.5 nm and provoked strong non-specific interactions with cells leading their rapid internalization. Therefore, to ensure proper folding of PMAO-based polymer into in a biocompatible single-chain NP, it is important to provide it with an appropriate hydrophobic/hydrophilic balance. Moreover, making it brightly fluorescent requires its modification with multiple fluorophores, which commonly leads to aggegation-caused quenching (ACQ).[24] Consequently, appropriate design of fluorophore should be made to minimize ACQ phenomena, such as introduction of bulky groups,[20,28,65-67] exploiting aggregation-induced emission (AIE)[21,22,68] and use of bulky hydrophobic counterions in case of ionic dyes.[69,70] Among existing fluorescent dyes, BODIPYs are one of the most popular because of their relatively high brightness, good photostability and versatile chemistry.[71] Presence of bulky groups has shown to improve the brightness of polymeric NPs.[67,72-74] However, so far BODIPY dyes or other high-performance fluorescent dyes had not been used for preparing single-chain fluorescent NPs.

In the present work, we developed the single chain polymer NPs that bear multiple covalently grafted BODIPY units. Strong PEGylation of PMAO was found essential to form single-chain NPs. Through a tailor-made design of BODIPY with bulky groups and the linker connecting it to the PMAO polymer, minimized ACQ was achieved, yielding ultra-small NPs brighter than QDs of the equivalent color. Finally, small size and strongly PEGylated surface ensured efficient spreading of NPs inside the cells after microinjection: they behaved similarly to red fluorescent proteins, while surpassing spreading of commercial quantum dots. Thus, the present design concepts enable preparation of protein-sized bright fluorescent NPs for cellular imaging applications.

Results and discussion

Effect of PEGylation. PEGylation is an essential approach to prevent nanoparticles from non-specific interactions, ensuring their "stealth" behavior.[75] PMAO is an alternating copolymer composed of maleic anhydrides (Figure 1) that readily react with amines to form stable amides. Primarily, we investigated the PMAO's reactivity and the effect of PEGylation level on the size of NPs assembled in water. To this endeavor, PMAO was reacted with an increasing amount (from 0 to 100 mol% with respect to reactive anhydrides) of Jeffamine® M-1000 (J-1000), a primary amine-terminated copolymer of propylene oxide (PO) and ethylene oxide (EO) with a PO/EO ratio of 3/19 ($H2N\text{-}(PO)_3\text{-}(EO)_{19}\text{-}OMe$). While $(EO)_{19}$ part ensures PEGylation, short $(PO)_3$ part may help to consolidate the hydrophobic part of future NPs. Poly(propylene oxide) fragment is present as a hydrophobic block in different Pluronic® surfactants, which are extensively used in biomedical applications.[76] The obtained polymers were analyzed by ^{1}H NMR which showed that the amount of PEG chains compared to the fixed amount of aliphatic chains was increasing according to the used feed ratio, thus demonstrating the reliability of the chemistry performed on PMAO (SI Figure S1). The polymers were dissolved in dioxane at a concentration of 2 mg/mL and then diluted in water to obtain NPs (100 µg/mL). The size of the formed NPs was assessed by DLS measurements. Although the increasing fraction of PEG provides polymers of higher molecular weight, small NPs (< 12 nm) were obtained starting from 20-50% PEGylation (SI Figure S2). We then hypothesized that the PEGylation decreased the hydrophobic nature of the amphiphilic polymer and therefore in water the PEGylated polymer molecules do not assemble together but fold into monomolecular (single-chain) micelles with a hydrophobic core of long hydrocarbon chains and a shell composed of PEG.

To confirm this hypothesis, three PMAO-based polymers, labeled with 5 mol% of an amino-BODIPY (BDP1), were synthesized: i) A non-PEGylated polymer where all the anhydride functions were hydrolyzed thus providing charged carboxylate groups, ii) A half-PEGylated one where all the anhydride functions were reacted with J-1000, thus still displaying carboxylate groups at the interface and iii) a fully-PEGylated polymer where all the anhydride functions were converted into diamides by condensing PMAO with J-1000 then using a coupling agent to react J-1000 with the formed carboxylate groups (Figure 1). The resulting polymers were purified by exclusion phase chromatography and analyzed by ^{1}H-NMR (SI Figure S3). For the half-PEGylated and the fully-PEGylated polymer, the PEGylation yields, determined by 1H NMR, were 96 and 88%, respectively (See SI for calculations).

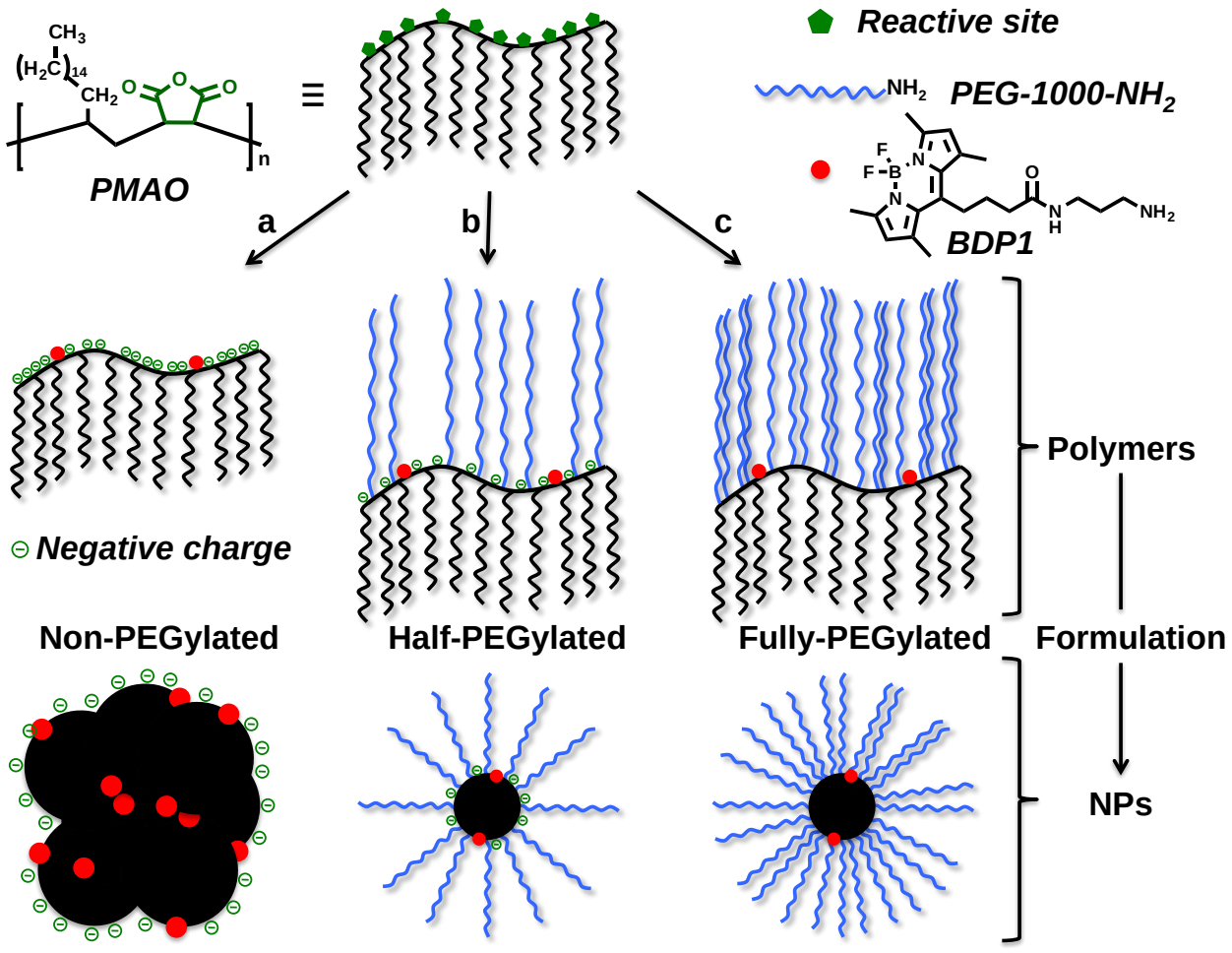

Figure 1. Synthesis of fluorescent amphiphilic polymers based on PMAO and their resulting NPs after formulation in water. a. BDP1, DIEA, DMF 60°C, then water. b. BDP1, DIEA then J-1000, DMF 60°C; c. BDP1, DIEA then J-1000, HATU, DMF 60°C.

The polymers were dissolved in dioxane (2 mg/mL) and then diluted in water to induce assembly of NPs (see materials and methods). The size of formed NPs was first measured by dynamic light scattering (DLS, Table 1). Although the non-PEGylated polymer gave NPs of 33.6 ± 2.4 nm ; the half-PEGylation led to ultra-small NPs of 9.7 ± 0.8 nm. Interestingly, the fully-PEGylated polymer provided slightly larger NPs of 11.5 ± 0.4 nm, probably due to an increased hydrodynamic diameter provoked by the denser PEG shell. According to ζ potential measurements (Table 1), the higher PEGylation level the lower negative charge displayed, clearly because the carboxylate groups were transformed into neutral amides. Indeed, whereas the non-PEGylated NPs displayed high ζ value of -51.6 mV, the half-PEGylation decreased it to -11.1 mV. The full PEGylation further reduced the zeta potential to a nearly neutral value (-2.7 ± 1.9).

Table 1. Physicochemical properties of the PMAO NPs. [a]

NPs	Size (nm)	PDI	ζ (mV)	λ_{Abs} (nm)	FMWH Abs (nm)	λ_{Em} (nm)	FMWH Em (nm)	QY (ϕ)
Non-PEGylated	33,6 ± 2.4	0.23	-51,6 ± 1.2	500	22	514	38	0.26
Half-PEGylated	9,7 ± 0.8	0.26	-11,1 ± 2.5	499	20	508	27	0.72
Fully-PEGylated	11,5 ± 0.4	0.45	-2,7 ± 1.9	499	20	507	26	0.79

[a] For sizes and ζ potential, the data were obtained from triplicates of three different formulation solutions (0.1 mg/mL). For spectroscopic data the polymer concentration was adjusted in order to fix the dye concentration at 2.5 μM, considering a molar extinction coefficient of 80,000 $M^{-1}cm^{-1}$ for a single BODIPY. The quantum yield was measured at 1 μM dye concentration using fluorescein (in 0.1 M NaOH, ϕ= 0.95) as a reference.

Consecutively, the NPs were imaged by transmission emission microscopy (Figure 2A and 2B). The non-PEGylated NPs displayed a round shape with sizes similar to those measured by DLS (32.4 ± 5.2). Fully-PEGylated NPs revealed ultrasmall round-shaped nanostructures of quite narrow distribution (9.8 ± 0.8 nm). These images tend to indicate that PEGylation in PMAO leads to formation of particles containing a single polymer molecule or only few of them. The round shape and small size of fully-PEGylated NPs also suggest that the polymers are folded into spherical (globular) structures rather than present in form of out-stretched polymer brush. Theoretically, the latter form would be 42-70 nm long considering all-*trans* configuration of the hydrocarbon backbone of PEGylated PMAO with molecular weight 30,000-50,000 Da (85-140 repetitive units).

Spectroscopic studies allowed to evaluating the number of polymer chains per particle. Upon PEGylation, convergent signs of de-aggregation of the dyes were observed: i) The blue shifted shoulder (at ~470 nm), which is a typical sign *H*-aggregates, decreased (Figure 2C), ii) the emission spectra shifted to the blue (7 nm between non- and fully-PEGylated NPs) accompanied by a decrease in the broadening (see FMWH values in Table 1 and Figure 2D), and finally iii) the measured quantum yields were significantly increased from 0.26 to 0.79 (Table 1). These observations suggest that high PEGylation level prevents form the formation of oligo-molecular NPs and thus favor the formation of monomolecular NPs where the fluorophores are better separated (Figure 1).

We also verified whether incorporation of BDP1 into the polymer affected BDP1 dye properties, which was done by comparing absorption and emission spectra of BDP1-amine (BDP1) and labelled fully-PEGylated polymer (5 mol% of BDP1) in organic solvents and water (SI Figure S4). In apolar dioxane and more polar PEG4, absorption and emission spectra of BDP1-polymer were

very similar to those of free dye BDP4-NH_2 (SI Figure S4), indicating that grafting to the polymer does not modify spectroscopic properties of the dye in solubilized form. Moreover, there was practically no spectral difference between these two organic solvents. However, in water, the absorption spectrum of the free dye (BPD1-NH_2) was blue shifted compared to organic solvents, and its emission spectrum was broadened, whereas the labelled polymer in water showed virtually the same spectral profile as in organic solvents (SI Figure S4). We can conclude that in water, the labelled polymer adapts a compact form that shields BDP1 dye from bulk water.

Next, the NPs were analyzed by electrophoresis. Owing to the high density of negative charges, the non-PEGylated NPs migrated fast to the anode, whereas the PEGylated NPs moved slower and displayed clear spots denoting their high homogeneity (Figure 2E). In the presence of BSA the non-PEGylated NPs migrated as a smear and reduced their migration towards the anode, probably because they interacted non-specifically with BSA. In sharp contrast, the PEGylated NPs did not change their migration profile when incubated in the presence of BSA, showing the absence of non-specific interactions. As another illustration of the PEGylation effect, the NPs were incubated for 1h in the presence of KB cells before being washed out (Figure 2F-H). The non-PEGylated NPs showed clear non-specific binding to the cells and aggregation due to precipitation in the high ionic strength medium (Opti-MEM). On the other hand, the cells incubated with PEGylated NPs did not display any fluorescence signal thus demonstrating the protecting effect of the PEG shell against non-specific interactions. In accordance with these results, cytotoxicity assays using MTT test revealed that unlike non-PEGylated polymer, PEGylated polymers did not affect the cells viability at concentrations up to 50 μg/mL (SI Figure S5).

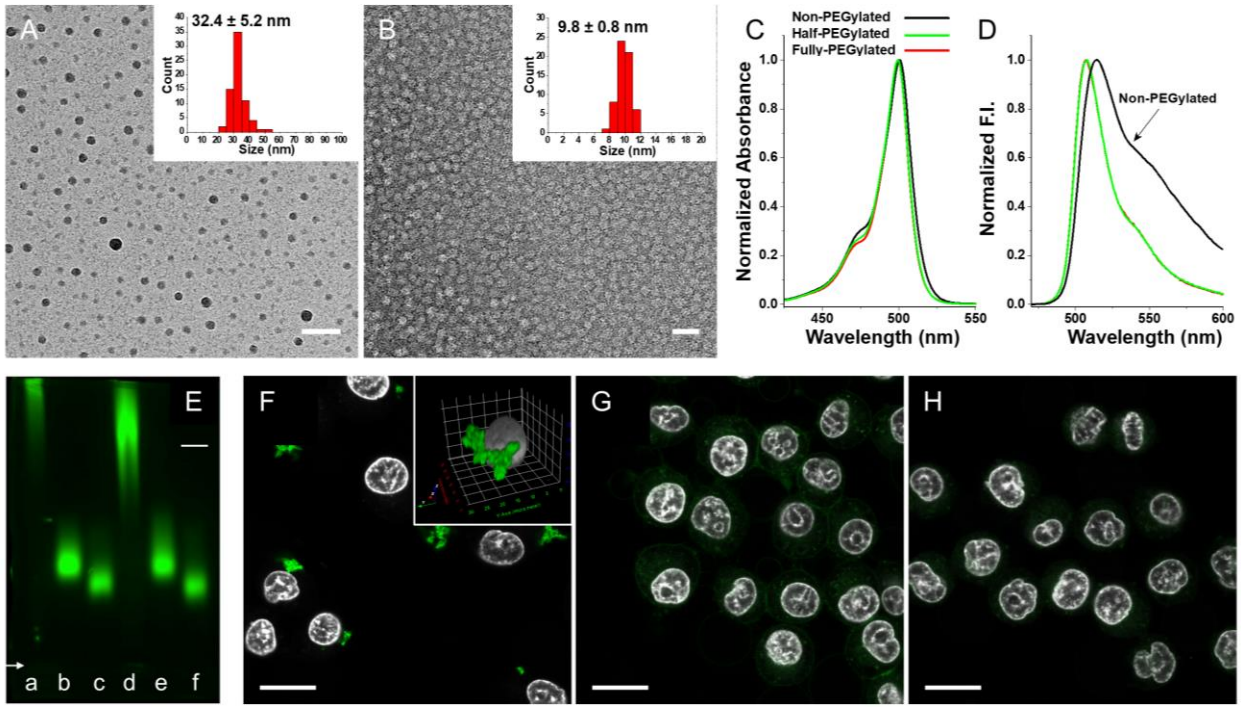

Figure 2. TEM images of non-PEGylated NPs (A) and fully-PEGylated NPs (B), scale bar is 150 nm and 30 nm respectively. Normalized absorption (C) and emission (D) spectra of the 3 different NPs in water (2.5 µM based on dye). (E) Agarose gel electrophoresis of non-PEGylated, half-PEGylated and fully-PEGylated NPs in TAE buffer (a, b and c respectively) and in the presence of 5 µM BSA (d, e and f respectively), 0.2 µg per well. The white arrow indicates the position of the wells. Scale bar is 0.5 cm. (F-H) Laser scanning confocal microscopy images of KB cells incubated for 1h in opti-MEM and in the presence of NPs: non-PEGylated (F), half-PEGylated (G) and fully-PEGylated (H). The concentration of polymer was adjusted in order to have 1 µM dye concentration. Inset in (F) is a 3D reconstruction of a cell containing the polymer. The nucleus (gray color) was stained with Hoechst (5 µg/mL). Excitation wavelength was 488 nm and emission was collected from 498 to 560 nm. The gain of the green channel's PMT was increased from 600 V for F to 1000 V for G and H in order to stress on the absence of signal. Scale bar is 20 µm.

FCS is a powerful spectroscopic technique providing simultaneously information on size, concentration, and brightness of fluorescent nanomaterials,[77,78] including polymeric NPs.[79] We used FCS to assess the behavior and composition of our NPs in water, PBS and PBS containing 10 µM BSA (Table 2). In water, the measured sizes were consistent with those obtained by DLS, namely 34, 8.6 and 11.4 nm for non-PEGylated, half-PEGylated and fully-PEGylated NPs respectively. In PBS, non-PEGylated NPs formed large aggregates (~7-fold larger than in water) due to their hydrophobic and charged nature. Interestingly, although the half-PEGylated NPs increased their size and decreased their concentration in PBS and in the presence of BSA, denoting a slight aggregation of the polymers molecules due to non-specific interactions, the fully-PEGylated NPs were negligibly affected (Table 2, SI Figure S6). This suggests that a high degree of PEGylation is necessary to lead to stealth and stable NPs with highly reduced non-specific interactions with proteins, which is in line with studies on other types of NPs.[75,80] The obtained result is also in good agreement with the electrophoresis data, where the effect of BSA was not observed in PEGylated NPs.

As we hypothesized previously, high PEGylation level might tend to form NPs composed of a small number of polymer molecules and even monomolecular NPs. As a first hint, a theoretical calculation based on i) the molecular weight of the fully-PEGylated PMAO polymers (~300,000 $g.mol^{-1}$), ii) the assumption that the formed NPs are spherical and iii) the assumption that the polymers have a density of ~1000 Kg/m^3, provided a theoretical size of 10.1 nm for a monomolecular NP (see SI for calculations). This value matches well the measured sizes of fully-PEGylated PMAO obtained by 3 different technics (DLS, TEM, FCS), supporting also organization of the polymer in the folded globular form (Figure 1). Second, FCS is perfectly adapted to confirm this hypothesis as it can measure the concentration of NPs. When

monomolecular NPs are obtained their concentration should be the same as the concentration of the polymer. The concentration of fluorophore was set at 1 µM by absorption spectroscopy. Since, on average, 7 dyes are displayed on a single polymer (5% of 140 units per polymer), the estimated concentration of single polymer molecules was 140 nM (1 µM divided by 7). For the PEGylated NPs, the concentration in water measured by FCS perfectly matched the estimated concentration of polymer molecules (Table 2), thus confirming our hypothesis on monomolecular nature of PEGylated PMAO based NPs.

FCS also provided information regarding the brightness of the formed NPs. Fluorescein was used as a reference (50 nM in NaOH 0.1 M, ϕ=0.95) and the brightness of the NPs was expressed in equivalent number of fluorescein molecules. Even though non-PEGylated NPs in water are composed of 24 polymers (~168 dyes) the brightness was equivalent to 23 fluorescein molecules due to high quenching of the fluorophores within the compacted polymers. On the other hand, half-PEGylated NPs and fully PEGylated NPs, composed of a single polymer, are as bright as 4 and 5 fluorescein molecules, respectively. Thus, the FCS data also confirmed that a high level of PEGylation enhanced the brightness of the obtained NPs.

Table 2. Physicochemical properties of the PMAO NPs obtained by FCS measurements.

Polymer	Conditions	Size (nm)[b]	[Particules] (nM)	Number of polymer per NP[c]	Relative brightness[d]
Non-PEGylated	Water	34.0	5.79	24.5	22.8
	PBS	261	0.133	1070	320
	10 µM BSA[a]	221	0.128	1110	413
Half-PEGylated	Water	8.6	143	0.994	4.00
	PBS	11.5	60.2	2.36	5.23
	10 µM BSA[a]	11.9	81.3	1.75	4.73
Fully-PEGylated	Water	11.4	138	1.03	4.98

PBS	12.2	110	1.29	4.98
10 µM BSA[a]	13.2	116	1.23	5.05

[a] In PBS. [b] Obtained considering the reference (fluorescein) being 1 nm. [c] The polymer concentration was adjusted to 1 µM fluorophore (corresponding to 140 nM polymer concentration). [d] Relative Brightness compared to the reference (fluorescein). The values were corrected according to the molar extinction coefficient values at the excitation wavelength (488 nm).

In contrast to the out-stretched configuration of a polymer brush, the folded monomolecular nanoparticle is expected to bear a hydrophobic core (Figure 1), similar to that of micelles made of surfactants. To evidence the presence of this core, we used a solvatochromic dye Nile Red, which is a common tool for identifying low polar environment of micelles[81] and single-chain polymeric NPs.[82] Fluorescence spectra of Nile Red at fixed concentration (200 nM) were recorded with addition of different concentrations of fully PEGylated PMAO polymer with 5 mol% BDP1 (SI Figure S7). A drastic increase in the fluorescence intensity of Nile Red was observed accompanied by ~30 nm blue shift of the emission band (SI Figure S7A,B,D). The increase in the intensity stabilized above 200 nM polymer concentration (SI Figure S7C), which corresponded well to 1/1 dye/polymer molar ratio. Below this concentration, multiple Nile Red molecules per particle can be present, which leads to dye self-quenching,[83] explaining lower intensity at lower polymer concentrations. On the other hand, the blue shifted emission of Nile Red at ~630 nm indicates the presence of a hydrophobic binding site in these NPs. We compared our NPs with micelles of Tween 80, having a hydrophobic core formed by hydrocarbon chains. Similar spectral changes were observed for Nile Red with addition of Tween 80, whereas above CMC (12 µM), blue shifted emission centered ~640 nm was observed (SI Figure S8). Our results suggest that in water the fully PEGylated polymer presents a hydrophobic binding site for a single emissive Nile Red molecule

and this site is even less polar than that in Tween 80 micelles, which support our model of the single-chain polymer folding into a particle with a apolar core. Lower polarity inside our NPs is probably related to their polymeric nature that drastically decreases dynamics of its amphiphilic units, in contrast to micelles based on small-molecule surfactants.

Effect of the linker. Encouraged by the interesting properties these NPs, we aimed at enhancing their brightness to the maximum. The brightness (B) of a NP composed of several fluorophores is defined by Equation 1 where n is the number of fluorophores that compose the NP, ε is the molar extinction coefficient value of the used fluorophore and ϕ is the measured quantum yield of the NP.

Eq. 1 $$B = n \times \varepsilon \times \phi$$

According to this equation, the brightness of a NP can theoretically be enhanced by increasing the fluorophore loading (n). However, concentrating fluorophores within a small volume tends to provoke *H*-aggregation by π-stacking of the fluorophores thus leading to the aggregation caused quenching (ACQ) phenomenon that lowers the quantum yield.[24] In order to prevent ACQ, we first investigated on the effect of the fluorophores' localization within the NP as the local concentration of the dye within the latter may vary (Figure 3). For this purpose, various linkers between the polymer and the fluorophore were used: i) a short linker that maintains the fluorophores at the interface ii) a long hydrocarbon chain (C12) that directs the fluorophores into the core of the NP by hydrophobic interactions with the hydrocarbon chains of PMAO and iii) a hydrophilic PEG_{12} that displays the fluorophore in the PEG shell of the NP. In addition to modifying the local dye concentration, these three different locations may alter hydration, polarity or viscosity of the dye environment that should also affect its quantum yield.

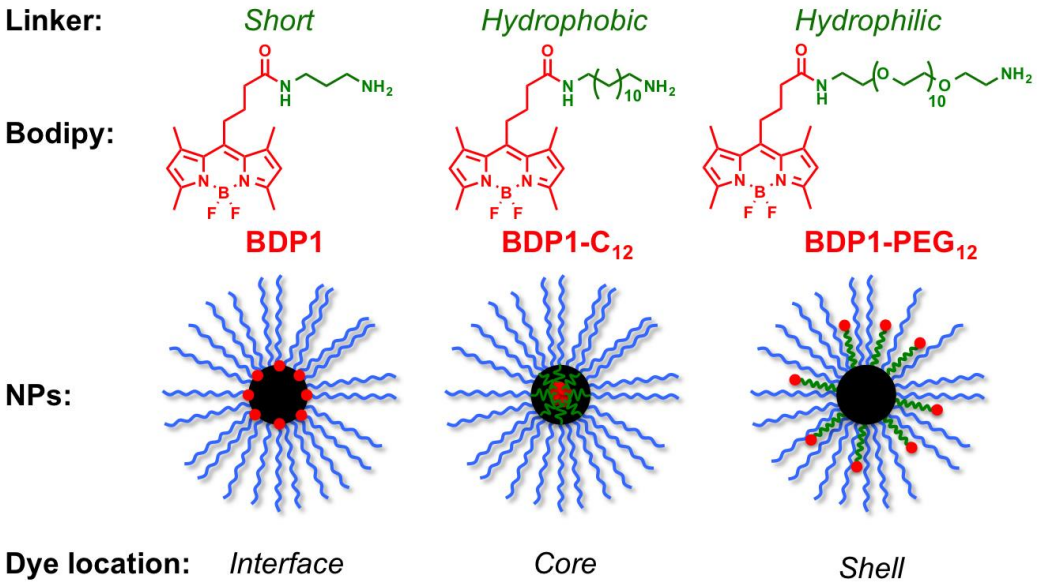

Figure 3. Synthesis of NPs displaying the fluorophores at different locations by means of linkers with various length and hydrophobicity.

PMAO was then reacted with the different amino-BODIPYs (Figure 3) at various loading percentage (from 2 to 50% of reactive sites) and was then fully PEGylated. The obtained polymers were purified and served to formulate the nanoparticles in water. The quenching phenomenon was monitored by the increase of the blue shifted shoulder on the absorption spectra (*H*-aggregation), the broadening of both absorption and fluorescence spectra as well as the decrease of the quantum yield values (Figure 4). The results showed that the contribution of the shoulder in the absorption spectra (Figure 4A-C) as well as the broadening of emission spectra (Figure 4 D-F) were less important when the fluorophores were used with PEG linker (*i.e.* located in the PEG shell). However, the decrease of quantum yield values upon dye functionalization percentage was fast in all cases and follows the same trend depicting a significant quenching of the dye regardless of the dyes' location (Figure 4G). Consequently, the brightness quickly reached a threshold below

400,000 $M^{-1}.cm^{-1}$ at only 10% loading (Figure 4H). It is noteworthy that when the BODIPYs were concentrated in the core of the NP using a hydrophobic linker (above 30% dye functionalization), the brightness slightly increased while the emission spectra broadened and shifts to the red. This could be attributed to complex forms of aggregation including emissive aggregation forms, such as *J*-aggregates.[84] Importantly, DLS measurements showed that small sizes of NPs were retained (10 to 14 nm) up to 40 % dye functionalization (Figure 4I). Additionally, NPs with 5% dye functionalization were compared by electrophoresis in the absence and presence of BSA (Figure S9). The NPs bearing the fluorophore through a short linker (*i.e.* dye located at the interface) were less smeary indicating their higher homogeneity. Moreover, in the presence of 5 μM BSA, these NPs were found to migrate in the same manner, as a single spot, whereas the NPs displaying the fluorophore at the core (with hydrophobic linker) or the PEG shell (PEG linker) started providing extra spots probably attributed to non-specific interactions with BSA. In the light of these results, the short linker was retained for the rest of our study.

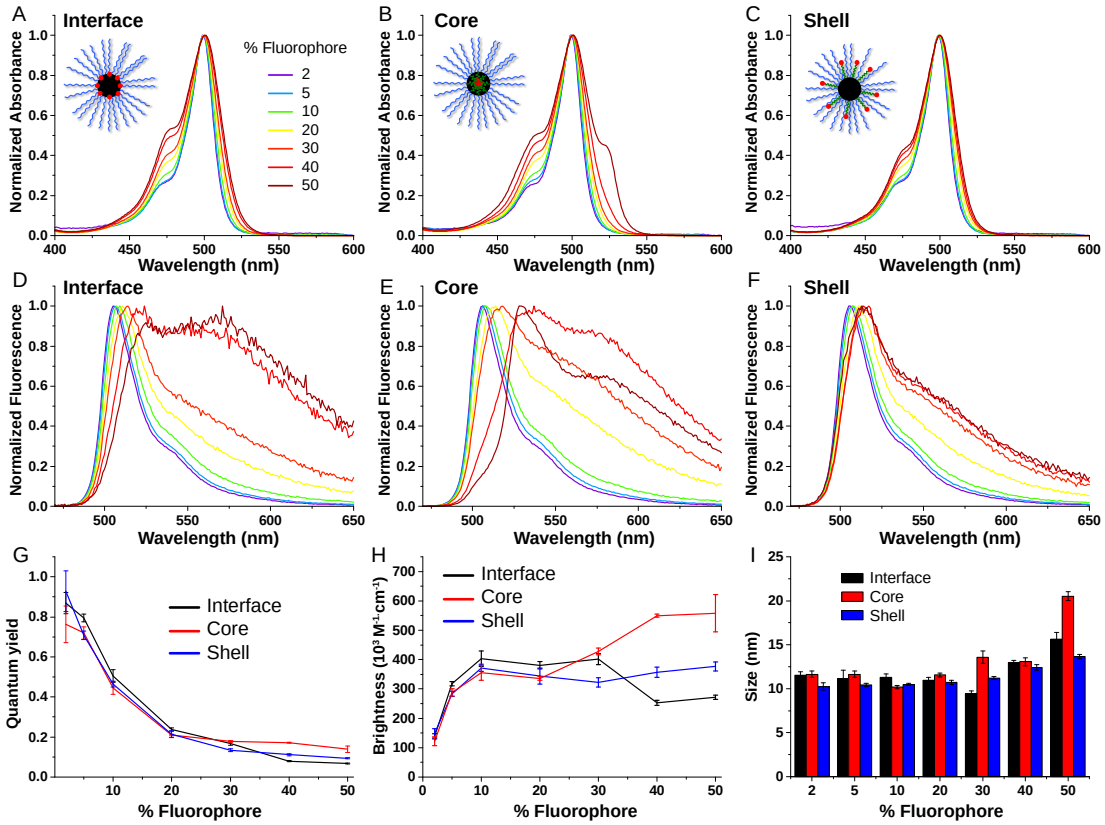

Figure 4. Characterization of NPs displaying the fluorophores: at the interface, the core and the PEG shell. Normalized absorption (A-C) and emission (D-F) spectra of NPs with increasing dye loading. Evolution of the quantum yield (G), brightness (H) and size (I) of the NPs with increasing dye loading. The brightness was calculated considering a monomolecular NPs and a ε value of the dye of 80,000 $M^{-1}.cm^{-1}$.

Effect of the dyes' bulkiness on the brightness of the NPs. The second approach to prevent aggregation-caused quenching and to improve the brightness of the NPs was to investigate on the BODIPY's bulkiness. Enhancing the bulkiness of fluorophores to prevent aggregation was successfully applied for different dyes, including BODIPY[67,72] and perylene diimide.[28,65,66] To this aim, we synthesized and used three new amino-functionalized BODIPYs with various bulkiness

patterns and with a short linker in order to localize the fluorophore at the interface (Figure 5). The bulkiness of the BODIPY was tuned by means of substitution at the *meso* position with a dimethyl phenyl group (BDP2) and at the *beta* positions with ethyl (BDP3) or diphenyl groups (BDP4). Here again, PMAO was reacted with the different amino-BODIPYs at various functionalization percentage and were then fully PEGylated.

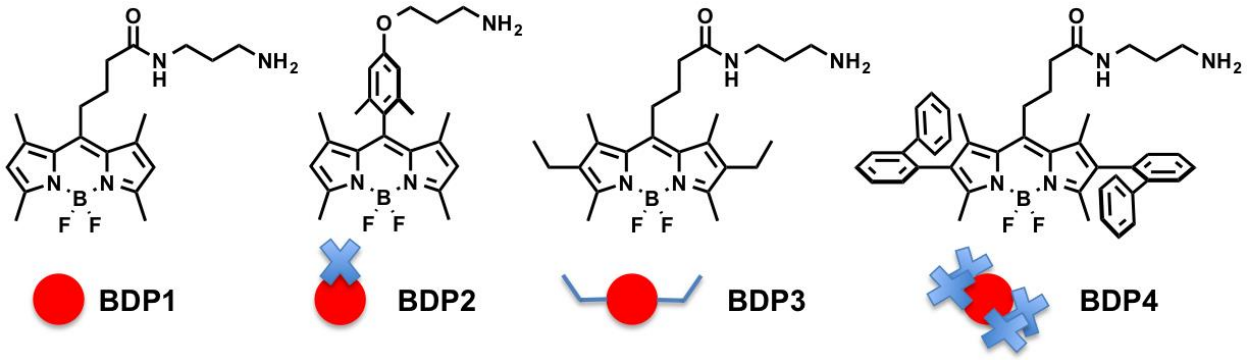

Figure 5. Synthesized amino-BODIPYs with various bulkiness patterns.

First, it is noteworthy that BODIPY dyes grafted to the polymer displayed different photophysical properties. From BDP2 to BDP4, longer absorption and emission wavelengths were observed (Figure 6) due to the increasing electron donor effect of the substituents in β position. Additionally, broadening of the spectra was observed which was ascribed to supplementary vibrational states due to the σ-bond rotations of the β substituents. Although broad spectra can be detrimental in multicolor imaging, where cross-talk can take place between the imaging channels, the broad absorption spectra of BDP4-based NPs can be an advantage as it can be excited by various excitation sources (*e.g.* 488 and 532 nm).

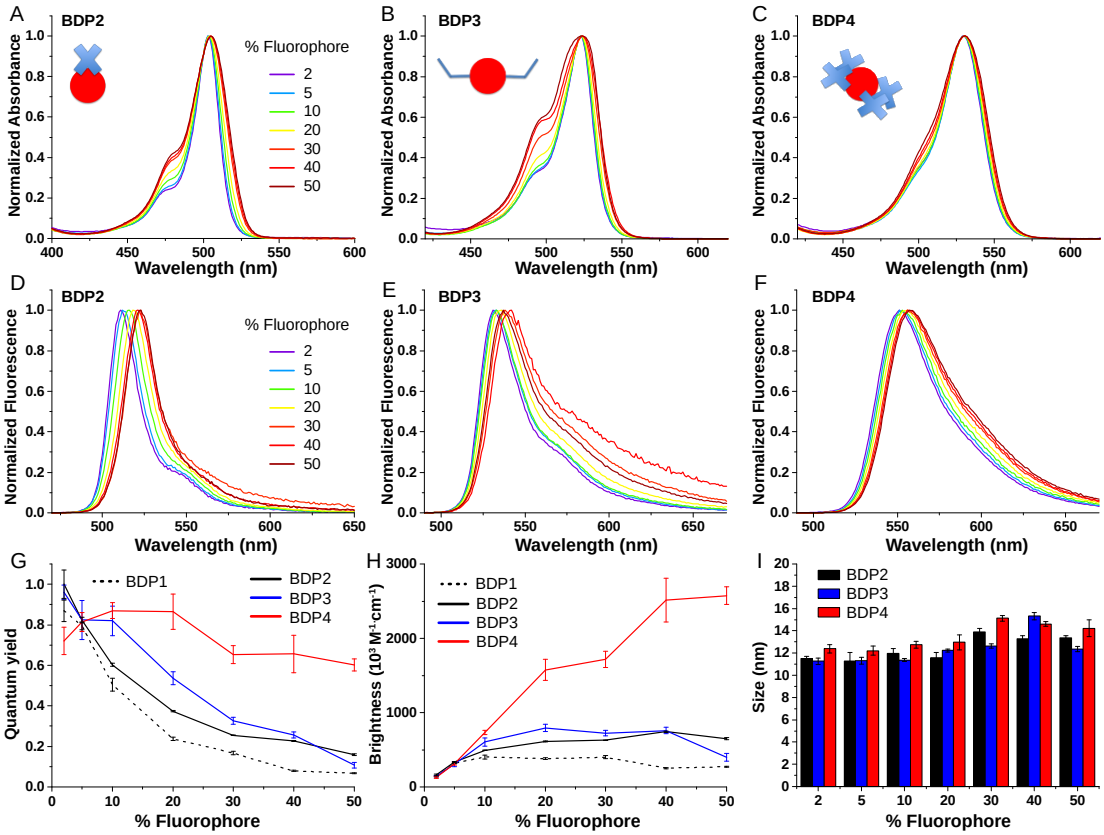

Figure 6. Characterization of NPs functionalized with BDP2, BDP3 and BDP4. Normalized absorption (A-C) and emission (D-F) spectra of NPs with increasing dye functionalization level. Evolution of quantum yield values (G), brightness (H) and size (I) of the NPs with increasing dye functionalization level. The brightness was calculated considering a monomolecular NP and a ε value of the dye of 80,000 M^{-1} cm^{-1}.

Further spectroscopic studies showed a dramatic influence of BODIPY's bulkiness on the self-quenching effect. In comparison to BDP1, bulkier BDP2 and BDP4 showed systematically lower increase in the short-wavelength shoulder (Figure 6A-C), and all three new derivatives BDP2-4 displayed narrower emission bands at high dye functionalization level (Figure 6D-F). In the case of the bulkiest fluorophore, BDP4, the spectroscopic changes upon increase in the dye

functionalization level were the smallest, showing the important effect of the bulky groups (Figure 6C and F). Even though the use of BDP2 and BDP3 helped in slowing down the quantum yield decrease compared to the initial BDP1, the brightness was limited to 800,000 M^{-1} cm^{-1} with 20% functionalization level using BDP3. The use of BDP4 allowed to maintaining quantum yield values above 0.6 regardless of the dye functionalization level thus leading to impressive brightness values up to ~2,500,000 M^{-1} cm^{-1} per monomolecular NP. We expect that the bulky groups effectively prevent BDP4 dyes from π-π stacking and formation of poorly emissive H-aggregates inside NPs.[24] The hydrodynamic diameters of the obtained NPs only slightly increased upon loading of the dye up to 14 nm and therefore allowed us to obtaining small and bright water soluble NPs. FCS measurements for BDP4 NPs (5 mo% loading) confirmed the small size, single-polymer chain nature of NPs and high particle brightness (SI Table S1, Figure S10). Moreover, similarly to NPs based on BDP1, BDP4 NPs showed high stability after incubation in PBS and BSA, because their size, concentration and brightness were close to those in water (SI Table S1, Figure S10).

In order to check whether the loading of BDP4 could affect the homogeneity of the formed NPs, the latter were analyzed by electrophoresis. The results confirmed the increasing brightness upon dye loading as well as a good homogeneity even at the highest dye loading (Figure 7A). Our brightest NPs were then imaged by single molecule microscopy and were compared to quantum dots that emit in the same wavelength range (QDot-585, streptavidin conjugate). Based on analysis of the average single particle brightness, the NPs loaded with 50% BDP4 was found to be 5.3 ± 1.3 fold brighter than QDots-585 under the same conditions of illumination, recording and processing (Figure 7B-E). The intensity distribution histograms confirmed the significantly higher brightness of our NPs *vs* QDots-585 (SI Figure S11), although the size distribution of the former was larger, probably related to the distribution of the PMAO polymer size and the dye grafting

ratio. The estimated brightness following equation (1) provided a value of 2.4×10^6 M^{-1} cm^{-1} for BDP4 NPs at an excitation wavelength at 532 nm. On the other hand, estimated brightness of QDot-585 at the same excitation wavelength is $\varepsilon \times QY = 310\,000$ M^{-1} $cm^{-1} \times 0.67 = 2.1 \times 10^5$ M^{-1} cm^{-1}.[85] Consequently, theoretically our NPs should be 11.4 times brighter, which is in line with 5.3-fold difference observed in the single-molecule microscopy. Somewhat lower than expected brightness of BDP4 NPs can be explained by the configuration of filters in the microscope, which collects light less efficiently in case of BDP4 NPs, because its emission band is closer to the excitation wavelength compared to that of QD585. It should be noted that, to keep the same imaging conditions for both types of NPs, QDs were not excited at UV-violet region, where they exhibit significantly higher extinction coefficients. Excitation of QDot-585 in this spectral region (around 400 nm) could result in the comparable brightness to our NPs, although this excitation region is less favorable for bioimaging because of phototoxicity and cell autofluorescence.

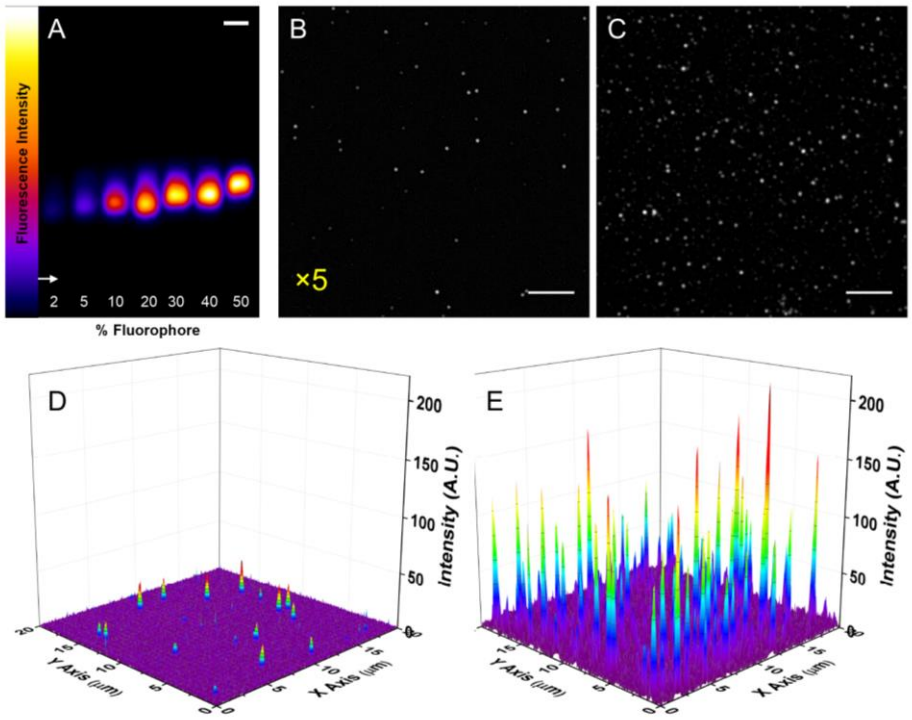

Figure 7. (A) Agarose gel (0.5 %) electrophoresis of NPs with increasing BDP4 loading (0.2 µg per well). The fluorescence intensity is color-coded as displayed. The white arrow indicates the level of the wells. Scale bar is 0.5 cm. Single particle fluorescence microscopy images (λEx= 532 nm, power density: 3 W cm^{-2}. Integration time was 20×100 ms) of QDots-585 streptavidin conjugate (B) and NPs containing 50% BDP4 (C). Scale bar is 5 µm. 3D Single particle fluorescence microscopy images of QDots-585 (D) and 50% BDP4 NPs (E).

Next, we aimed at studying the photostability of our NPs. First, we compared NPs at various BDP1 loading and as a standard we used fluorescent polystyrene NPs (FluoroSpheres^{TM} 505/515, ThermoFisher) emitting in the same spectral range. As expected FluoroSpheres^{TM} displayed robust photostability, whereas BDP1-loaded NPs displayed lower stability losing up to 50% of the fluorescence intensity (SI Figure S12). A decrease in the photostability was observed with increase in the dye loading. This phenomenon might be attributed to intermolecular reactions in the excited state which is promoted by the close proximity of the fluorophores. Similar loss of photostability were observed earlier for polymeric NPs loaded with perylenediimide[65] and rhodamine[69] dyes. In a second step, we studied the BDP4-loaded NPs (SI Figure S13), where a correlation between dye loading and photostability was also observed. However, compared to BDP1, BDP4-loaded NPs were significantly more photostable with similar photostability of our NPs with 20 mol% BDP4 and QDots-585. This photostability improvement might be ascribed to the difference in the bulkiness between BDP4 and BDP1. Indeed, the steric hindrance of the dyes prevents from ACQ and collisions that might promote reaction and then bleaching of the dye. However, at the highest loading (50 mol%), the NPs displayed impressive decay of fluorescence intensity depicting a low

photostability (SI Figure S13). The latter indicates that a compromise should be found between dye loading and photostability to achieve the best performance.

Finally, we wondered if such a high degree of dye functionalization could be detrimental for the cell viability. Therefore, MTT test was performed on NPs loaded with 50% BDP4 and showed no apparent cytotoxicity (Figure S5).

Intracellular behavior of NPs. As demonstrated above, we developed ultrabright NPs with size comparable to large proteins. These NPs and proteins share another common point as they both can display reduced non-specific interaction in biological media. Indeed, proteins are able to circulate freely in the cell until they rich their biological target. Here, we compared the cytosolic behavior of our NPs with the one of proteins. To do so, HeLa cells were co-microinjected with green emitting NPs (20% BDP1 functionalization, 10 nm size, see Figure 4). BDP1 was chosen instead of other BDP to avoid cross talk in the red channel) together with mCherry (3.5 nm size, 28.8 KDa), a red emitting fluorescent protein (Figure 8A-C). Moreover, analogous experiment was done by co-microinjecting the same NPs with far red emitting Qdots-655 as a bright water-soluble nanoparticles standard (Figure 8E-G, and SI Figure S14). We selected streptavidin-coated QDots-655, so that their size (20 nm diameter, according to the manufacturer) is ~2-fold larger compared to the BDP1 NPs. First, the fluorescence microscopy images showed that our NPs (green signal) occupied the whole cell surface denoting a smooth distribution within the cytoplasm with no sign of aggregates. Then, we compared the distribution of the green signal from our NPs with the one of the red signal from the co-injected fluorescent protein or QDots-655. When our NPs were co-injected with mCherry, their fluorescence signals overlaid in a quite homogeneous manner (Figure 8C) and their fluorescence intensity decrease similarly (down to 60% for mCherry and 50% for

NPs) from the injection point to the extremities of the cell (Figure 8D). In sharp contrast, the QDots-655 signal decreased rapidly when it got away from the injection point and the fluorescence intensity decreased down to 20% at the extremities of the cell (Figure 8H, SI Figure S14). These results suggest that the herein developed fluorescent NPs have similar intracellular spreading compared to a small hydrophilic protein, probably because of their small (10 nm) size and thick PEG shell that protects NPs from non-specific interactions thus insuring them a fast progression in the cytoplasm. Less efficient intracellular spreading of the QDs compared to our NPs is probably related to the larger size of streptavidin-coated QDots-655. This observation is in line with recent works showing that increase in size of NPs in the range 10-40 nm can drastically decrease their intracellular diffusion and spreading in the cytosol.[3,4] Thus, the ultra-small size and strong PEGylation make our single-chain polymeric NPs compatible with intracellular applications.

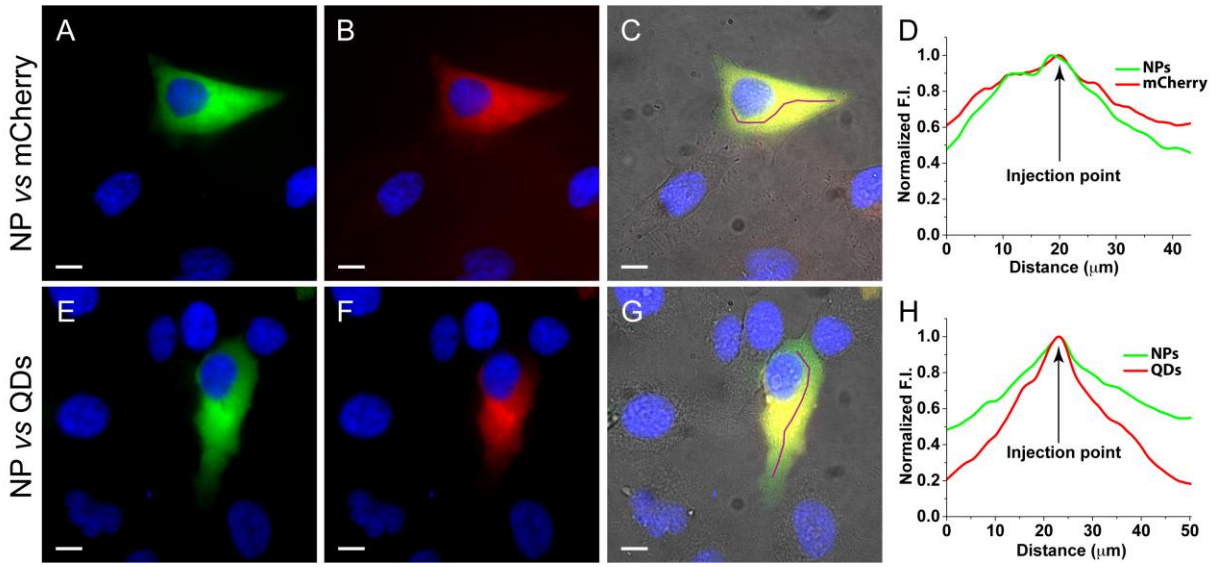

Figure 8. Comparison of intracellular distribution of BDP1-based NPs with that of a fluorescent protein (mCherry) and quantum dots (QDots-655). Co-injection in HeLa cells of NPs (20% BDP1, 0.33 μM) with mCherry (1.75 μM) (A, B, C) or with QDots-655 Streptavidin Conjugate (0.05 μM + BSA 5 mg/mL) (E, F and G). NPs are in green (A, E), mCherry and Qdots-655 (QDs) are in red

(B and F respectively). C and G are the merge of A and B and E and F respectively with the brightfield channel. D and H are the plots of normalized intensity corresponding to the line in C and G respectively. Scale bar is 10 μm.

Conclusion

Replacing fluorescent dyes with bright nanoparticles can boost performance of fluorescence sensing and imaging. However, nanoparticles are much larger than molecules and their non-specific interactions and homogeneity is difficult to control. To address this issue, we herein propose to explore a biomimetic phenomenon of single-chain polymer folding.[36-41] In contrast to previously reported fluorescently-labeled water-soluble hydrophilic polymers,[86,87] we designed fluorescent amphiphilic alternating polymers that fold into globular monomolecular nanoparticle, similarly to proteins. The folded micelle-like globular structures of the polymer is expected to ensure compact uniform structure with alkyl chains in the hydrophobic core and tightly packed polar shell at the surface to prevent non-specific interactions. The design is based on highly PEGylated poly(maleic anhydride-alt-1-octadecene) functionalized with large amount (up to 50 mol%) of BODIPY dyes. We found that strong PEGylation rate is required to ensure folding into the monomolecular particles. Fluorescence correlation spectroscopy suggested that the obtained NPs are stable in physiological salt conditions and do not exhibit non-specific interactions with proteins, probably due to highly dense PEG shell. Then, we tested linkers of different length and polarity connecting BODIPY to the polymer and found that short medium-polar linker ensured small size and good fluorescent properties of NPs, which suggest that the particle interface is the most optimal location of the dye. Importantly, incorporation of bulky groups into BODIPY dye prevented it from *H*-aggregation inside the particle, which allowed us to dramatically enhance its fluorescence quantum yield for high dye grafting ratio. The obtained NPs reached an impressive brightness value of 2,500,000 M^{-1} cm^{-1} with a hydrodynamic diameter of 14 nm and were found to be 5-fold brighter than QDot-585 (~20 nm) at 532 nm excitation, according to single-particle fluorescence microscopy. Finally, when microinjected in cells, these small and stealth NPs diffused

more evenly inside the cytosol than QDots, highlighting the importance of the size for reaching sterically hindered compartments of the cytosol. The intracellular spreading of our NPs was similar to that of a red fluorescent protein, which shows that they can be considered as artificial protein analogues, compatible with the intracellular applications. The proposed concept of fluorescent monomolecular polymeric NPs enables preparation of nanomaterials with controlled small and uniform size and bright fluorescence for numerous bioimaging applications.

Materials & Methods

Synthesis. All starting materials for synthesis were purchased from Alfa Aesar, Sigma Aldrich or TCI Europe and used as received unless stated otherwise. PMAO was purchased from sigma Aldrich, Jeffamine® was kindly offered by Huntsman International. NMR spectra were recorded on a Bruker Avance III 400 MHz spectrometer. Mass spectra were obtained using an Agilent Q-TOF 6520 mass spectrometer. Protocol of synthesis of all new compounds as well as NMR and mass spectra can be found in the supporting information.

Formulation of the nanoparticles. In an eppendorf was placed 50 μL (100 μg of polymer) of stock solution of amphiphilic polymer in dioxane at a concentration of 2 $mg.mL^{-1}$. 950 □L of miliQ water or PBS was quickly added and the solution was vigorously mixed with help of pipetting followed by vortexing for 5 s. The final concentration of polymer is 0.1 $mg.mL^{-1}$.

Spectroscopy. The water used for spectroscopy was Milli-Q water (Millipore), all the solvents were spectro grade. Absorption and emission spectra were recorded on a Cary 400 Scan ultraviolet–visible spectrophotometer (Varian) and a FluoroMax-4 spectrofluorometer (Horiba Jobin Yvon) equipped with a thermostated cell compartment, respectively. For standard recording of fluorescence spectra, the emission was collected 10 nm after the excitation wavelength. All the spectra were corrected from wavelength-dependent response of the detector. Quantum yields were determined at optical density ≤0.1 by comparison with a reference according to their excitation and emission wavelengths: Fluorescein in (0.1 M NaOH, ϕ= 0.95)[88] or Rhodamine 6G in water (ϕ= 0.95).[89]

Photostability assay. Aqueous solutions of NPs were placed in a 50 μL quartz cuvette and the entire solution was continuously irradiated at 486 nm for 20 min with slit opening at 16 nm. The fluorescence intensity was monitored at the maximum emission wavelength determined by emission spectra prior to kinetic measurements. For fair comparison, the concentrations were adjusted to obtain identical optical density of 0.015 at the excitation wavelength of 486 nm. Emission slit opening was set to obtain optimal signal.

Fluorescence Correlation Spectroscopy (FCS). FCS measurements were performed on a home-built confocal set-up based on a Nikon inverted microscope with a Nikon 60x 1.2NA water immersion objective.[4] Excitation was provided by a cw laser diode (488 nm, Oxxius). For the fluorescence signal detection, a fibered Avalanche Photodiode (APD, PerkinElmer, Fremont, CA) connected to an on-line hardware correlator (ALV7000-USB, ALV GmbH, Germany) was used. Before the APD, the fluorescence signal was filtered through a 405/488/ 532/635 nm BrightLines quad-edge laser-grade dichroic (Semrock, NY) and ET525/50 single band-pass filter (Chroma Corp., Rockingham, VT). The fluorescence signal was further processed by an ALV7002/USB digital correlator (ALV, Langen, Germany). Typical acquisition time was 5 min (10-30 scans) with an excitation power of 0.5 mW at the laser output level.

The data were analyzed using the PyCorrFit software.[90] Assuming that NPs diffuse freely in a Gaussian excitation volume and taking into account triplet blinking, the correlation function, G(τ), calculated from the fluorescence fluctuations was fitted according to equation (1):[91]

$$G(\tau)=\frac{1}{N}\,\frac{(1-F+Fe^{\frac{\tau}{\tau_F}})}{(1-F)}\,(1+\frac{\tau}{\tau d})^{-1}\,(1+\frac{1}{S^2}\frac{\tau}{\tau d})^{-1/2} \quad (1)$$

where τ_d is the diffusion time, N is the mean number of fluorescent species within the excitation volume, and S is the ratio between the axial and lateral radii of the excitation volume; F is the fraction of emissive species that have entered the triplet state and τ_F is the corresponding triplet

state relaxation time. The measurements were done with respect to a reference dye fluorescein (FL) (Sigma-Aldrich) at 50 nM concentration in 0.1 mM NaOH. The hydrodynamic diameter, d, of NPs was calculated as $d_{NPs} = \tau_{d(NPs)}/\tau_{d(FL)} \times d_{FL}$, where d_{FL} is the hydrodynamic diameter of fluorescein (1.0 nm). The concentration of NPs was calculated from the number of species by $C_{NPs} = N_{NPs}/N_{FL} \times C_{FL}$, where N_{NPs} and N_{FL} are number of emissive species of NPs and fluorescein, respectively, and C_{FL} is fluorescein concentration (50 nM).

200 µL of each samples were placed in a 96-well plate. Generally, FCS measurements were done 30 min after dilution of NPs in the corresponding medium (water, PBS or PBS with BSA). The concentration of polymer was adjusted to 1 µM BODIPY using 80,000 M^{-1} cm^{-1} as molar extinction coefficient value, therefore providing a polymer concentration of 140 nM (7 fluorophores per polymer).

Single-particle microscopy. Prior to imaging the surface of 8 wells-Lab-Tek chambered coverglass was treated for 1 h with an aqueous solution of KOH (1 M). Then, the wells' surface was extensively rinsed with ultrapure water and incubated with PEI solution (1 mg/mL in tris buffer) at RT for 15 min followed by rinsing with ultrapure water. The solutions of NPs were added and allowed to stay at RT for 30 minutes in the dark before the being removed and replaced by mQ water. Single-particle measurements were performed in the total internal reflection (TIRF) mode using a Nikon Ti-E inverted microscope with a 100× objective (Apo TIRF, oil, NA 1.49, Nikon). The excitation was provided by OXXIUS laser at 532 nm with 3.0 W/cm^2 excitation power density. The presented images were an average of the first 20 frames (recorded at a 100 ms integration time. The single-particle analysis was performed using Fiji software, similarly to the previously described protocol.[79] Briefly, particle locations were detected through a Fiji routine applied to a projection (maximum intensity) of 100 frames using an appropriate threshold. The

mean intensities of circular regions of interest with a diameter of 5 pixels around the found particle locations were then measured. Background subtraction was then achieved by measuring the mean intensities in circular bands around the circular regions of interest and subtracting them. Finally, integrated intensity in all circular regions of interest was calculated and used for building the histograms of particle intensities. For BDP4 NPs and QDots-585, 150 and 50 particles were analyzed, respectively. Average intensity (± sem) of the two types of NPs was compared.

Dynamic Light Scattering and Zeta potential. The size and the surface Zeta potential (ζ) of the NPs were measured three times from three independent formulations in milliQ water at 25°C using a Malvern Zetasizer Nano ZSP (Malvern, U.K.). DLS laser was 633 nm.

Transmission Electron Microscopy. 5 µL of the formulation solution were deposited onto carbon-coated copper-rhodium electron microscopy grids that were used following amylamine glow-discharge. The grids were then treated for 1 min with a 2 % uranyl acetate solution for staining and observed with a Philips CM120 transmission electron microscope equipped with a LaB_6 filament and operating at 100 kV. Areas covered with NPs of interest were recorded on a Peltier cooled CCD camera (Model 794, Gatan, Pleasanton, CA). Image analysis was performed using the ImageJ software.

Gel electrophoresis. The electrophoresis was performed on an agarose gel (0.5%) in TAE buffer (TRIS, acetate, EDTA). In each well, 20 µL of a solution of NPs (0.01 mg/mL in water) were cautiously added (0.2 µg polymer per well). The gel was gently covered with TAE then a tension of 125 V was applied for one hour. The gels were visualized with an ImageQuant LAS 4000 (GE

Healthcare Life Sciences) using Cy2 (473 nm) or Cy3 (532 nm) excitation channels and by acquiring 10 images with an exposition time of 10 seconds. The images were treated with ImageJ.

Cytotoxicity assay. Cytotoxicity assay of the NPs was quantified by the MTT assay (3-(4,5-dimethylthiazol-2-yl)-2,5-diphenyltetrazolium bromide). A total of $1x10^4$ HeLa (ATCC® CCL-2™) cells/well were seeded in a 96-well plate 24 h prior to the cytotoxicity assay in Dulbecco's Modified Eagle Medium (Gibco Lifetechnologies -DMEM) complemented with 10% fetal bovine serum, Gentamicin (100 µg/mL), L-Glutamine (2 mM), non-essential amino acids (1 mM), MEM vitamin solution (1%) and were incubated in a 5% CO_2 incubator at 37°C. After medium removal, an amount of 100 µL DMEM containing NPs at various concentrations (10 to 50 µg polymer/mL) was added to the cells and incubated for 24 h at 37°C (5% CO_2). As control, for each 96-well plate, the cells were incubated with DMEM containing the same percentage of dioxane as the solution with the tested NPs or with triton X-100 0.1% as a positive control of cytotoxicity. After 24h of a dye incubation, the medium was replaced by 100 µL of a mixture containing DMEM and MTT solution (diluted in PBS beforehand) and the cells were incubated for 4 h at 37°C. Then, 75 µL of the mixture was replaced by 50 µL of DMSO (100%) and gently shaken for 15 min at room temperature in order to dissolve the insoluble purple formazan reduced in the living cells. The absorbance at 540 nm was measured (absorbance of the NPs at 540 nm were taken into account). Each concentration of dye was tested in sextuplicate in 3 independent assays. For each concentration, we calculated the percentage of cell viability in reference of the control DMEM and dioxane.

Cell imaging. KB cells (ATCC® CCL-17™) and HeLa (ATCC® CCL-2™) were grown in minimum essential medium (MEM, Gibco-Invitrogen) with 10% fetal bovine serum (FBS, Lonza),

1% non-essential amino acids (Gibco-Invitrogen), 1% MEM vitamin solution (Gibco-Invitrogen), 1% L-Glutamine (Sigma Aldrich) and 0.1% antibiotic solution (gentamicin, Sigma-Aldrich) at 37° C in humidified atmosphere containing 5% CO_2. Cells were seeded onto a chambered coverglass (IBiDi®) at a density of 5×10^4 cells/well 24 h before the microscopy measurement. For imaging, the culture medium was removed and the attached cells were washed with Opti-MEM (Gibco–Invitrogen). Next, the cells were incubated in Opti-MEM with Hoechst (5 μg/mL) to stain the nuclei and in the presence of the NPs (1 μM dye concentration) for 1 h, the living cells were washed three times with HBSS and visualized in HBSS. Confocal microscopy experiments were performed by using a Leica TCS SPE-II with HXC PL APO 63x/1.40 OIL CS objective.

Microinjection. Cells were microinjected using a Femtojet® 4i device (Eppendorf), with femtotip II (Eppendorf) containing: NPs (0.33 μM) + mCherry (BioVision, 1.75 μM) or NPs (0.33 μM) + Qdot™ 655 Streptavidin Conjugate (Thermo Fisher, 0.05 μM) + BSA (5 mg/mL). Microinjection parameters: Pi=80 [hPa]; Ti=0.5 [s]; Pc=10 [hPa]. The images were acquired in epi-fluorescence mode with a Nikon Ti-E inverted microscope, equipped with CFI Plan Apo × 60 oil (NA = 1.4) objective, and a Hamamatsu Orca Flash 4 sCMOS camera. The acquisition settings were: Hoechst (ex. 395 nm, em. 475±50 nm), NPs (ex: 470 nm, em: 531±40 nm); Qdot™ 655 and mCherry (ex: 550 nm, em: 595±40 nm). The images were recorded using NIS Elements and then processed with Icy software.[6]

ASSOCIATED CONTENT

Supporting Information. Protocols of synthesis, caracterizations, calculations, cytotoxicity, and control experiments can be found in the Supporting Information. The Supporting Information is available free of charge at https://pubs.acs.org/doi

AUTHOR INFORMATION

Corresponding Authors

- Dr. Mayeul Collot: mayeul.collot@unistar.fr
- Dr. Andrey Klymchenko: andrey.klymchenko@unistra.fr

Author Contributions

The manuscript was written through contributions of all authors. All authors have given approval to the final version of the manuscript.

Notes

The authors declare no competing financial interest.

ACKNOWLEDGMENTS

This work was supported by the European Research Council ERC Consolidator grant BrightSens 648528. The authors would like to thank Christine Ruhlmann and Dr. Andreas Reisch for performing the TEM images, Fatima Menadi for her assistance with some experiments, Nina Melnychuk for help with the image analysis, and the Huntsman Corporation for kindly providing Jeffamine M-1000.

REFERENCES

1. Wolfbeis, O. S. An Overview of Nanoparticles Commonly Used in Fluorescent Bioimaging. *Chem. Soc. Rev.* **2015**, *44*, 4743.
2. Howes, P. D.; Chandrawati, R.; Stevens, M. M. Colloidal Nanoparticles as Advanced Biological Sensors. *Science* **2014**, *346*, 1247390.
3. Liu, Y.; Le, P.; Lim, S. J.; Ma, L.; Sarkar, S.; Han, Z. Y.; Murphy, S. J.; Kosari, F.; Vasmatzis, G.; Cheville, J. C.; Smith, A. M. Enhanced Mrna Fish with Compact Quantum Dots. *Nat. Commun.* **2018**, *9*, 8.
4. Reisch, A.; Heimburger, D.; Ernst, P.; Runser, A.; Didier, P.; Dujardin, D.; Klymchenko, A. S. Protein-Sized Dye-Loaded Polymer Nanoparticles for Free Particle Diffusion in Cytosol. *Adv. Funct. Mater.* **2018**, *28*, 10.
5. Virant, D.; Traenkle, B.; Maier, J.; Kaiser, P. D.; Bodenhöfer, M.; Schmees, C.; Vojnovic, I.; Pisak-Lukáts, B.; Endesfelder, U.; Rothbauer, U. A Peptide Tag-Specific Nanobody Enables High-Quality Labeling for Dstorm Imaging. *Nat. Commun.* **2018**, *9*, 930.
6. Cabral, H.; Matsumoto, Y.; Mizuno, K.; Chen, Q.; Murakami, M.; Kimura, M.; Terada, Y.; Kano, M. R.; Miyazono, K.; Uesaka, M.; Nishiyama, N.; Kataoka, K. Accumulation of Sub-100 Nm Polymeric Micelles in Poorly Permeable Tumours Depends on Size. *Nat. Nanotechnol.* **2011**, *6*, 815.
7. Zhang, C.; Li, C.; Liu, Y.; Zhang, J.; Bao, C.; Liang, S.; Wang, Q.; Yang, Y.; Fu, H.; Wang, K.; Cui, D. Gold Nanoclusters-Based Nanoprobes for Simultaneous Fluorescence Imaging and Targeted Photodynamic Therapy with Superior Penetration and Retention Behavior in Tumors. *Adv. Funct. Mater.* **2015**, *25*, 1314.
8. Alivisatos, A. P. Semiconductor Clusters, Nanocrystals, and Quantum Dots. *Science* **1996**, *271*, 933.
9. Wegner, K. D.; Hildebrandt, N. Quantum Dots: Bright and Versatile *in Vitro* and *in Vivo* Fluorescence Imaging Biosensors. *Chem. Soc. Rev.* **2015**, *44*, 4792.
10. Medintz, I. L.; Uyeda, H. T.; Goldman, E. R.; Mattoussi, H. Quantum Dot Bioconjugates for Imaging, Labelling and Sensing. *Nat. Mater.* **2005**, *4*, 435.
11. Montalti, M.; Prodi, L.; Rampazzo, E.; Zaccheroni, N. Dye-Doped Silica Nanoparticles as Luminescent Organized Systems for Nanomedicine. *Chem. Soc. Rev.* **2014**, *43*, 4243.
12. Colombe, C.; Le Guevel, X.; Martin-Serrano, A.; Henry, M.; Porret, E.; Comby-Zerbino, C.; Antoine, R.; Atallah, I.; Busser, B.; Coll, J. L.; Righini, C. A.; Sancey, L. Gold Nanoclusters as a Contrast Agent for Image-Guided Surgery of Head and Neck Tumors. *Nanomed.-Nanotechnol. Biol. Med.* **2019**, *20*, 11.
13. Ding, H.; Yu, S. B.; Wei, J. S.; Xiong, H. M. Full-Color Light-Emitting Carbon Dots with a Surface-State-Controlled Luminescence Mechanism. *ACS Nano* **2016**, *10*, 484.
14. Lim, S. Y.; Shen, W.; Gao, Z. Q. Carbon Quantum Dots and Their Applications. *Chem. Soc. Rev.* **2015**, *44*, 362.
15. Feliu, N.; Docter, D.; Heine, M.; del Pino, P.; Ashraf, S.; Kolosnjaj-Tabi, J.; Macchiarini, P.; Nielsen, P.; Alloyeau, D.; Gazeau, F.; Stauber, R. H.; Parak, W. J. *in Vivo* Degeneration and the Fate of Inorganic Nanoparticles. *Chem. Soc. Rev.* **2016**, *45*, 2440.
16. Pecher, J.; Mecking, S. Nanoparticles of Conjugated Polymers. *Chem. Rev.* **2010**, *110*, 6260.
17. Wu, C.; Chiu, D. T. Highly Fluorescent Semiconducting Polymer Dots for Biology and Medicine. *Angew. Chem. Int. Ed.* **2013**, *52*, 3086.

18. Wu, C.; Bull, B.; Szymanski, C.; Christensen, K.; McNeill, J. Multicolor Conjugated Polymer Dots for Biological Fluorescence Imaging. *ACS Nano* **2008**, *2*, 2415.
19. Kaeser, A.; Schenning, A. P. H. J. Fluorescent Nanoparticles Based on Self-Assembled Pi-Conjugated Systems. *Adv. Mater.* **2010**, *22*, 2985.
20. Gorl, D.; Zhang, X.; Wurthner, F. Molecular Assemblies of Perylene Bisimide Dyes in Water. *Angew. Chem. Int. Ed.* **2012**, *51*, 6328.
21. Hong, Y. N.; Lam, J. W. Y.; Tang, B. Z. Aggregation-Induced Emission. *Chem. Soc. Rev.* **2011**, *40*, 5361.
22. Mei, J.; Leung, N. L. C.; Kwok, R. T. K.; Lam, J. W. Y.; Tang, B. Z. Aggregation-Induced Emission: Together We Shine, United We Soar! *Chem. Rev.* **2015**, *115*, 11718.
23. Li, K.; Liu, B. Polymer-Encapsulated Organic Nanoparticles for Fluorescence and Photoacoustic Imaging. *Chem. Soc. Rev.* **2014**, *43*, 6570.
24. Reisch, A.; Klymchenko, A. S. Fluorescent Polymer Nanoparticles Based on Dyes: Seeking Brighter Tools for Bioimaging. *Small* **2016**, *12*, 1968.
25. Peng, H.-S.; Chiu, D. T. Soft Fluorescent Nanomaterials for Biological and Biomedical Imaging. *Chem. Soc. Rev.* **2015**, *44*, 4699.
26. Guan, W. J.; Zhou, W. J.; Lu, C.; Tang, B. Z. Synthesis and Design of Aggregation-Induced Emission Surfactants: Direct Observation of Micelle Transitions and Microemulsion Droplets. *Angew. Chem. Int. Ed.* **2015**, *54*, 15160.
27. Petkau, K.; Kaeser, A.; Fischer, I.; Brunsveld, L.; Schenning, A. Pre- and Postfunctionalized Self-Assembled Pi-Conjugated Fluorescent Organic Nanoparticles for Dual Targeting. *J. Am. Chem. Soc.* **2011**, *133*, 17063.
28. Zhang, X.; Chen, Z. J.; Wurthner, F. Morphology Control of Fluorescent Nanoaggregates by Co-Self-Assembly of Wedge- and Dumbbell-Shaped Amphiphilic Perylene Bisimides. *J. Am. Chem. Soc.* **2007**, *129*, 4886.
29. Shulov, I.; Rodik, R. V.; Arntz, Y.; Reisch, A.; Kalchenko, V. I.; Klymchenko, A. S. Protein-Sized Bright Fluorogenic Nanoparticles Based on Cross-Linked Calixarene Micelles with Cyanine Corona. *Angew. Chem. Int. Ed.* **2016**, *55*, 15884.
30. Shulov, I.; Arntz, Y.; Mely, Y.; Pivovarenko, V. G.; Klymchenko, A. S. Non-Coordinating Anions Assemble Cyanine Amphiphiles into Ultra-Small Fluorescent Nanoparticles. *Chem. Commun.* **2016**, *52*, 7962.
31. Wu, W. C.; Chen, C. Y.; Tian, Y. Q.; Jang, S. H.; Hong, Y. N.; Liu, Y.; Hu, R. R.; Tang, B. Z.; Lee, Y. T.; Chen, C. T.; Chen, W. C.; Jen, A. K. Y. Enhancement of Aggregation-Induced Emission in Dye-Encapsulating Polymeric Micelles for Bioimaging. *Adv. Funct. Mater.* **2010**, *20*, 1413.
32. Jones, M. C.; Leroux, J. C. Polymeric Micelles - A New Generation of Colloidal Drug Carriers. *Eur. J. Pharm. Biopharm.* **1999**, *48*, 101.
33. Nishiyama, N.; Kataoka, K. Current State, Achievements, and Future Prospects of Polymeric Micelles as Nanocarriers for Drug and Gene Delivery. *Pharmacol. Ther.* **2006**, *112*, 630.
34. Dobson, C. M. Protein Folding and Misfolding. *Nature* **2003**, *426*, 884.
35. Nicholls, A.; Sharp, K. A.; Honig, B. Protein Folding and Association - Insights from the Interfacial and Thermodynamic Properties of Hydrocarbons. *Proteins* **1991**, *11*, 281.
36. Schmidt, B.; Fechler, N.; Falkenhagen, J.; Lutz, J. F. Controlled Folding of Synthetic Polymer Chains through the Formation of Positionable Covalent Bridges. *Nat. Chem.* **2011**, *3*, 234.
37. Altintas, O.; Lejeune, E.; Gerstel, P.; Barner-Kowollik, C. Bioinspired Dual Self-Folding of Single Polymer Chains *via* Reversible Hydrogen Bonding. *Polym. Chem.* **2012**, *3*, 640.

38. Altintas, O.; Barner-Kowollik, C. Single Chain Folding of Synthetic Polymers by Covalent and Non-Covalent Interactions: Current Status and Future Perspectives. *Macromol. Rapid Commun.* **2012**, *33*, 958.
39. Lo Verso, F.; Pomposo, J. A.; Colmenero, J.; Moreno, A. J. Multi-Orthogonal Folding of Single Polymer Chains into Soft Nanoparticles. *Soft Matter* **2014**, *10*, 4813.
40. Altintas, O.; Barner-Kowollik, C. Single-Chain Folding of Synthetic Polymers: A Critical Update. *Macromol. Rapid Commun.* **2016**, *37*, 29.
41. Hanlon, A. M.; Lyon, C. K.; Berda, E. B. What Is Next in Single-Chain Nanoparticles? *Macromolecules* **2016**, *49*, 2.
42. Koda, Y.; Terashima, T.; Sawamoto, M. Multimode Self-Folding Polymers *via* Reversible and Thermoresponsive Self-Assembly of Amphiphilic/Fluorous Random Copolymers. *Macromolecules* **2016**, *49*, 4534.
43. Matsumoto, K.; Terashima, T.; Sugita, T.; Takenaka, M.; Sawamoto, M. Amphiphilic Random Copolymers with Hydrophobic/Hydrogen-Bonding Urea Pendants: Self-Folding Polymers in Aqueous and Organic Media. *Macromolecules* **2016**, *49*, 7917.
44. Terashima, T.; Sugita, T.; Sawamoto, M. Single-Chain Crosslinked Star Polymers *via* Intramolecular Crosslinking of Self-Folding Amphiphilic Copolymers in Water. *Polym. J.* **2015**, *47*, 667.
45. Berda, E. B.; Foster, E. J.; Meijer, E. W. Toward Controlling Folding in Synthetic Polymers: Fabricating and Characterizing Supramolecular Single-Chain Nanoparticles. *Macromolecules* **2010**, *43*, 1430.
46. Heiler, C.; Offenloch, J. T.; Blasco, E.; Barner-Kowollik, C. Photochemically Induced Folding of Single Chain Polymer Nanoparticles in Water. *ACS Macro Lett.* **2017**, *6*, 56.
47. Terashima, T.; Mes, T.; De Greef, T. F. A.; Gillissen, M. A. J.; Besenius, P.; Palmans, A. R. A.; Meijer, E. W. Single-Chain Folding of Polymers for Catalytic Systems in Water. *J. Am. Chem. Soc.* **2011**, *133*, 4742.
48. Sanchez-Sanchez, A.; Arbe, A.; Colmenero, J.; Pomposo, J. A. Metallo-Folded Single-Chain Nanoparticles with Catalytic Selectivity. *ACS Macro Lett.* **2014**, *3*, 439.
49. Rothfuss, H.; Knofel, N. D.; Roesky, P. W.; Barner-Kowollik, C. Single-Chain Nanoparticles as Catalytic Nanoreactors. *J. Am. Chem. Soc.* **2018**, *140*, 5875.
50. Perez-Baena, I.; Barroso-Bujans, F.; Gasser, U.; Arbe, A.; Moreno, A. J.; Colmenero, J.; Pomposo, J. A. Endowing Single-Chain Polymer Nanoparticles with Enzyme-Mimetic Activity. *ACS Macro Lett.* **2013**, *2*, 775.
51. Song, C. F.; Li, L. Y.; Dai, L. Z.; Thayumanavan, S. Responsive Single-Chain Polymer Nanoparticles with Host-Guest Features. *Polym. Chem.* **2015**, *6*, 4828.
52. Liu, Y. L.; Pauloehrl, T.; Presolski, S. I.; Albertazzi, L.; Palmans, A. R. A.; Meijer, E. W. Modular Synthetic Platform for the Construction of Functional Single-Chain Polymeric Nanoparticles: From Aqueous Catalysis to Photosensitization. *J. Am. Chem. Soc.* **2015**, *137*, 13096.
53. Sanchez-Sanchez, A.; Akbari, S.; Moreno, A. J.; Lo Verso, F.; Arbe, A.; Colmenero, J.; Pomposo, J. A. Design and Preparation of Single-Chain Nanocarriers Mimicking Disordered Proteins for Combined Delivery of Dermal Bioactive Cargos. *Macromol. Rapid Commun.* **2013**, *34*, 1681.
54. De-La-Cuesta, J.; Gonzalez, E.; Pomposo, J. A. Advances in Fluorescent Single-Chain Nanoparticles. *Molecules* **2017**, *22*.

55. De-La-Cuesta, J.; Pomposo, J. A. Photoactivation of Aggregation-Induced Emission Molecules for Fast and Efficient Synthesis of Highly Fluorescent Single-Chain Nanoparticles. *ACS Omega* **2018**, *3*, 15193.
56. Wang, P.; Pu, H. T.; Ge, J.; Jin, M.; Pan, H. Y.; Chang, Z. H.; Wan, D. C. Fluorescence-Labeled Hydrophilic Nanoparticles via Single-Chain Folding. *Mater. Lett.* **2014**, *132*, 102.
57. Di Corato, R.; Quarta, A.; Piacenza, P.; Ragusa, A.; Figuerola, A.; Buonsanti, R.; Cingolani, R.; Manna, L.; Pellegrino, T. Water Solubilization of Hydrophobic Nanocrystals by Means of Poly(Maleic Anhydride-Alt-1-Octadecene). *J. Mater. Chem.* **2008**, *18*, 1991.
58. Galiyeva, P.; Alem, H.; Rinnert, H.; Balan, L.; Blanchard, S.; Medjahdi, G.; Uralbekov, B.; Schneider, R. Highly Fluorescent, Color Tunable and Magnetic Quaternary Ag-in-Mn-Zn-S Quantum Dots. *Inorg. Chem. Front.* **2019**, *6*, 1422.
59. Peng, E.; Shi, E.; Choo, G.; Tan, C. S. H.; Tang, X. S.; Sheng, Y.; Xue, J. M. Multifunctional Pegylated Nanoclusters for Biomedical Applications. *Nanoscale* **2013**, *5*, 5994.
60. Yang, J.; Dave, S. R.; Gao, X. H. Quantum Dot Nanobarcodes: Epitaxial Assembly of Nanoparticle-Polymer Complexes in Homogeneous Solution. *J. Am. Chem. Soc.* **2008**, *130*, 5286.
61. Plohl, O.; Kralj, S.; Majaron, B.; Frohlich, E.; Ponikvar-Svet, M.; Makovec, D.; Lisjak, D. Amphiphilic Coatings for the Protection of Upconverting Nanoparticles against Dissolution in Aqueous Media. *Dalton Trans.* **2017**, *46*, 6975.
62. Guryev, E. L.; Shilyagina, N. Y.; Kostyuk, A. B.; Sencha, L. M.; Balalaeva, I. V.; Vodeneev, V. A.; Kutova, O. M.; Lyubeshkin, A. V.; Yakubovskaya, R. I.; Pankratov, A. A.; Ingel, F. I.; Novik, T. S.; Deyev, S. M.; Ermilov, S. A.; Zvyagin, A. V. Preclinical Study of Biofunctional Polymer-Coated Upconversion Nanoparticles. *Toxicol. Sci.* **2019**, *170*, 123.
63. Dung, N. T.; Long, N. V.; Tam, L. T. T.; Nam, P. H.; Tung, L. D.; Phuc, N. X.; Lu, L. T.; Thanh, N. T. K. High Magnetisation, Monodisperse and Water-Dispersible Cofe@Pt Core/Shell Nanoparticles. *Nanoscale* **2017**, *9*, 8952.
64. Lee, Y. D.; Lim, C. K.; Kim, S.; Kwon, I. C.; Kim, J. Squaraine-Doped Functional Nanoprobes: Lipophilically Protected Near-Infrared Fluorescence for Bioimaging. *Adv. Funct. Mater.* **2010**, *20*, 2786.
65. Trofymchuk, K.; Reisch, A.; Shulov, I.; Mely, Y.; Klymchenko, A. S. Tuning the Color and Photostability of Perylene Diimides inside Polymer Nanoparticles: Towards Biodegradable Substitutes of Quantum Dots. *Nanoscale* **2014**, *6*, 12934.
66. Tian, Z.; Shaller, A. D.; Li, A. D. Q. Twisted Perylene Dyes Enable Highly Fluorescent and Photostable Nanoparticles. *Chem. Commun.* **2009**, 180.
67. Grazon, C.; Rieger, J.; Charleux, B.; Clavier, G.; Meallet-Renault, R. Ultrabright Bodipy-Tagged Polystyrene Nanoparticles: Study of Concentration Effect on Photophysical Properties. *J. Phys. Chem. C* **2014**, *118*, 13945.
68. Ding, D.; Li, K.; Liu, B.; Tang, B. Z. Bioprobes Based on Aie Fluorogens. *Acc. Chem. Res.* **2013**, *46*, 2441.
69. Reisch, A.; Didier, P.; Richert, L.; Oncul, S.; Arntz, Y.; Mely, Y.; Klymchenko, A. S. Collective Fluorescence Switching of Counterion-Assembled Dyes in Polymer Nanoparticles. *Nat. Commun.* **2014**, *5*, 4089.
70. Andreiuk, B.; Reisch, A.; Bernhardt, E.; Klymchenko, A. S. Fighting Aggregation-Caused Quenching and Leakage of Dyes in Fluorescent Polymer Nanoparticles: Universal Role of Counterion. *Chem.-Asian J.* **2019**, *14*, 836.
71. Ulrich, G.; Ziessel, R.; Harriman, A. The Chemistry of Fluorescent Bodipy Dyes: Versatility Unsurpassed. *Angew. Chem. Int. Ed.* **2008**, *47*, 1184.

72. Vu, T. T.; Badré, S.; Dumas-Verdes, C.; Vachon, J.-J.; Julien, C.; Audebert, P.; Senotrusova, E. Y.; Schmidt, E. Y.; Trofimov, B. A.; Pansu, R. B.; Clavier, G.; Méallet-Renault, R. New Hindered Bodipy Derivatives: Solution and Amorphous State Fluorescence Properties. *J. Phys. Chem. C* **2009**, *113*, 11844.
73. Trofymchuk, K.; Valanciunaite, J.; Andreiuk, B.; Reisch, A.; Collot, M.; Klymchenko, A. S. Bodipy-Loaded Polymer Nanoparticles: Chemical Structure of Cargo Defines Leakage from Nanocarrier in Living Cells. *J. Mat. Chem. B* **2019**, *7*, 5199.
74. Grazon, C.; Rieger, J.; Méallet-Renault, R.; Charleux, B.; Clavier, G. Ultrabright Fluorescent Polymeric Nanoparticles Made from a New Family of Bodipy Monomers. *Macromolecules* **2013**, *46*, 5167.
75. Pelaz, B.; del Pino, P.; Maffre, P.; Hartmann, R.; Gallego, M.; Rivera-Fernandez, S.; de la Fuente, J. M.; Nienhaus, G. U.; Parak, W. J. Surface Functionalization of Nanoparticles with Polyethylene Glycol: Effects on Protein Adsorption and Cellular Uptake. *ACS Nano* **2015**, *9*, 6996.
76. Pitto-Barry, A.; Barry, N. P. E. Pluronic® Block-Copolymers in Medicine: From Chemical and Biological Versatility to Rationalisation and Clinical Advances. *Polym. Chem.* **2014**, *5*, 3291.
77. Woll, D. Fluorescence Correlation Spectroscopy in Polymer Science. *RSC Adv.* **2014**, *4*, 2447.
78. Klymchenko, A. S.; Roger, E.; Anton, N.; Anton, H.; Shulov, I.; Vermot, J.; Mely, Y.; Vandamme, T. F. Highly Lipophilic Fluorescent Dyes in Nano-Emulsions: Towards Bright Non-Leaking Nano-Droplets. *RSC Adv.* **2012**, *2*, 11876.
79. Reisch, A.; Runser, A.; Arntz, Y.; Mély, Y.; Klymchenko, A. S. Charge-Controlled Nanoprecipitation as a Modular Approach to Ultrasmall Polymer Nanocarriers: Making Bright and Stable Nanoparticles. *ACS Nano* **2015**, *9*, 5104.
80. Ke, P. C.; Lin, S.; Parak, W. J.; Davis, T. P.; Caruso, F. A Decade of the Protein Corona. *ACS Nano* **2017**, *11*, 11773.
81. Stuart, M. C. A.; van de Pas, J. C.; Engberts, J. The Use of Nile Red to Monitor the Aggregation Behavior in Ternary Surfactant-Water-Organic Solvent Systems. *J. Phys. Org. Chem.* **2005**, *18*, 929.
82. Chan, D.; Yu, A. C.; Appel, E. A. Single-Chain Polymeric Nanocarriers: A Platform for Determining Structure-Function Correlations in the Delivery of Molecular Cargo. *Biomacromolecules* **2017**, *18*, 1434.
83. Kurniasih, I. N.; Liang, H.; Mohr, P. C.; Khot, G.; Rabe, J. P.; Mohr, A. Nile Red Dye in Aqueous Surfactant and Micellar Solution. *Langmuir* **2015**, *31*, 2639.
84. Wurthner, F.; Kaiser, T. E.; Saha-Moller, C. R. J-Aggregates: From Serendipitous Discovery to Supramolecular Engineering of Functional Dye Materials. *Angew. Chem. Int. Ed.* **2011**, *50*, 3376.
85. Shulov, I.; Oncul, S.; Reisch, A.; Arntz, Y.; Collot, M.; Mely, Y.; Klymchenko, A. Fluorinated Counterion-Enhanced Emission of Rhodamine Aggregates: Ultrabright Nanoparticles for Bioimaging and Light-Harvesting. *Nanoscale* **2015**, *7*, 18198.
86. Beija, M.; Charreyre, M. T.; Martinho, J. M. G. Dye-Labelled Polymer Chains at Specific Sites: Synthesis by Living/Controlled Polymerization. *Prog. Polym. Sci.* **2011**, *36*, 568.
87. Fouz, M. F.; Mukumoto, K.; Averick, S.; Molinar, O.; McCartney, B. M.; Matyjaszewski, K.; Armitage, B. A.; Das, S. R. Bright Fluorescent Nanotags from Bottlebrush Polymers with DNA-Tipped Bristles. *ACS Cent. Sci.* **2015**, *1*, 431.
88. Brannon, J. H.; Magde, D. Absolute Quantum Yield Determination by Thermal Blooming - Fluorescein. *J. Phys. Chem.* **1978**, *82*, 705.

89. Magde, D.; Rojas, G. E.; Seybold, P. G. Solvent Dependence of the Fluorescence Lifetimes of Xanthene Dyes. *Photochem. Photobiol.* **1999**, *70*, 737.
90. Muller, P.; Schwille, P.; Weidemann, T. Pycorrfit-Generic Data Evaluation for Fluorescence Correlation Spectroscopy. *Bioinformatics* **2014**, *30*, 2532.
91. Widengren, J.; Mets, U.; Rigler, R. Fluorescence Correlation Spectroscopy of Triplet-States in Solution - A Theoretical and Experimental-Study. *J. Phys. Chem.* **1995**, *99*, 13368.